Delft University of Technology

Quantum Dots in an InSb Two-Dimensional Electron Gas

Kulesh, Ivan; Ke, Chung Ting; Thomas, Candice; Karwal, Saurabh; Moehle, Christian M.; Metti, Sara; Kallaher, Ray; Gardner, Geoffrey C.; Manfra, Michael J.; Goswami, Srijit

Important note
To cite this publication, please use the final published version (if applicable).
Please check the document version above.

Quantum Dots in an InSb Two-Dimensional Electron Gas

Ivan Kulesh[1,*] Chung Ting Ke,[1] Candice Thomas,[2,3] Saurabh Karwal,[4] Christian M. Moehle,[1]
Sara Metti,[3,5] Ray Kallaher,[3,6] Geoffrey C. Gardner,[3,6] Michael J. Manfra,[2,3,5,6,7] and Srijit Goswami[1,†]

[1]*QuTech and Kavli Institute of Nanoscience, Delft University of Technology, 2600 GA Delft, Netherlands*
[2]*Department of Physics and Astronomy, Purdue University, West Lafayette, Indiana 47907, USA*
[3]*Birck Nanotechnology Center, Purdue University, West Lafayette, Indiana 47907, USA*
[4]*QuTech and Netherlands Organization for Applied Scientific Research (TNO), 2628 CK Delft, Netherlands*
[5]*School of Electrical and Computer Engineering, Purdue University, West Lafayette, Indiana 47907, USA*
[6]*Microsoft Quantum Purdue, Purdue University, West Lafayette, Indiana 47907, USA*
[7]*School of Materials Engineering, Purdue University, West Lafayette, Indiana 47907, USA*

Indium-antimonide (InSb) two-dimensional electron gases (2DEGs) have a unique combination of material properties: high electron mobility, a strong spin-orbit interaction, a large Landé g factor, and a small effective mass. This makes them an attractive platform to explore a variety of mesoscopic phenomena ranging from spintronics to topological superconductivity. However, there exist limited studies of quantum confined systems in these 2DEGs, often attributed to charge instabilities and gate drifts. We overcome this by removing the δ-doping layer from the heterostructure and induce carriers electrostatically. This allows us to perform a detailed study of stable gate-defined quantum dots in InSb 2DEGs. We demonstrate two distinct strategies for carrier confinement and study the charge stability of the dots. The small effective mass results in a relatively large single-particle spacing, allowing for the observation of an even-odd variation in the addition energy. By tracking the Coulomb oscillations in a parallel magnetic field, we determine the ground-state spin configuration and show that the large g factor (approximately 30) results in a singlet-triplet transition at magnetic fields as low as 0.3 T.

Mesoscopic devices can be made in a two-dimensional electron gas (2DEG) using electrical gates to confine charge carriers, thus reducing the degrees of freedom. The extreme case is the zero-dimensional system, a quantum dot (QD). QDs have been used to explore a wide range of quantum phenomena [1–3] and are emerging as a platform for quantum computing [4–6] and quantum simulations [7–9]. QDs in materials with a strong spin-orbit interaction have important applications in the field of topological superconductivity. They can be used to realize Majorana zero modes in QD chains [10] and are essential elements for the readout and manipulation of topological qubits [11,12].

InSb is a promising material in this regard, with a high carrier mobility, a large g factor, and a strong spin-orbit interaction [13–16]. QDs have been extensively studied in InSb nanowires [17–19] and, more recently, in InSb nanoflakes [20]. However, despite the clear benefits of scalability offered by InSb 2DEGs, experimental reports of confined systems in these quantum wells are scarce

[14,21,22]. Thus far, most studies of InSb 2DEGs have been limited to heterostructures where carriers are generated in the quantum well via remote δ-doping layers. Such doped 2DEGs are known to suffer from charge instability and gate drifts, which are particularly detrimental to the study of nanostructures.

Here, we show that the removal of doping layers enables the realization of highly stable gate-defined QDs in InSb 2DEGs. We study two different QD designs on deep and shallow undoped quantum wells. In all measured devices, the charge-stability diagrams show well-defined Coulomb diamonds and excited states. We find that the small effective mass of InSb results in a large separation between single-particle levels, enabling the observation of an even-odd periodicity in the Coulomb peak spacing. Studying the evolution of these peaks in magnetic field allows us to extract the g factor and determine the parity of ground states (GSs).

The QDs are fabricated on InSb quantum wells grown by molecular-beam epitaxy on GaAs (100) substrates. Electronic confinement in the quantum well is obtained with the growth of (Al,In)Sb barriers on either side [see Fig. 1(a)]. The Supplemental Material [23] provides

*I.Kulesh-1@tudelft.nl
†S.Goswami@tudelft.nl

(a)

(b) Barrier Contacts **(d)**
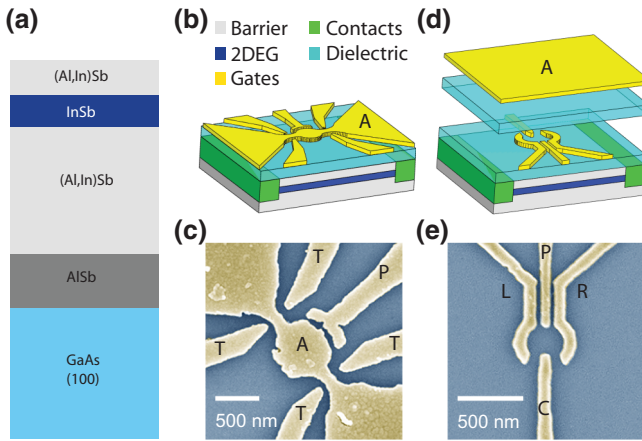2DEG Dielectric
Gates

(c)

(e)

FIG. 1. (a) The layer stack of the InSb/(Al,In)Sb heterostructure. (b) A sketch of the single-layer and (d) the double-layer types of design. A positive voltage is applied to gates A populating charge carriers, while the other gates are energized with negative voltages and control the system as explained in the text. (c) A false-color scanning electron micrograph of the single-layer dot and (e) the double-layer dot prior to the second gate-layer deposition.

further details on the growth, the layer stack, and the characterization of the wafers, including their density, mobility, and accumulation curves. The key difference here, as compared to previous studies [13,14,21,22,24], is the absence of a δ-doping layer, which is typically inserted above the quantum well to generate carriers. Instead, we populate the well by applying positive voltages to an accumulation gate, an approach widely used in other semiconductor-2DEG materials [25–27].

Figures 1(b) and 1(d) show schematics of QDs with either a single or a double layer of gates. The fabrication flow is similar for both types of designs (for more details, see the Supplemental Material [23]). We first isolate lithographically defined mesas using wet chemical etching with a citric acid solution. Ti/Au ohmic contacts are made to the buried quantum well after removal of the native oxide via passivation in ammonium-polysulfide solution [28,29]. The entire structure is then covered by 40 nm of aluminum oxide [30] with atomic layer deposition (ALD), followed by the deposition of Ti/Au top gates. Figures 1(c) and 1(e) show scanning electron micrographs at this stage for the single- and double-layer devices, respectively. While the fabrication of single-layer QDs ends here, the double-layer devices require an additional layer of aluminum oxide, followed by a global-accumulation gate (A).

The single-layer QD has a local-accumulation gate (A) that, when energized with a positive voltage, creates a populated 2DEG region following the shape of the gate. The tunnel gates (T) are then used to tune the barriers and the plunger gate (P) controls the chemical potential of the dot. For double-layer QDs, carriers are induced via the

TABLE I. An overview of the samples studied in this work.

Device	Doping	QW depth (nm)	Gate layers
S1	No	40	2
S2	No	10	2
S3	No	10	1
S4	Yes	40	1

global-accumulation gate. The QD confinement potential and tunnel barriers are controlled via the fine gates labeled left (L), right (R), and central (C) and the plunger (P) again tunes the chemical potential. While the first design is simpler and offers the flexibility to integrate with other mesoscopic systems, the latter provides better control on the dot size and occupation, with the possibility of depleting it to the few-electron regime [31]. Here, we report results on three QDs in undoped wafers (S1, S2, and S3) and one on a doped wafer (S4) for comparison. The relevant design type and top-barrier thickness are summarized in Table I. All measurements are performed in a refrigerator with a base temperature of 300 mK. We use standard lock-in techniques with an ac excitation of 10–20 μV and measure the differential conductance G.

We first compare the stability of QDs fabricated on undoped (S1) and doped (S4) quantum wells. In the latter, the Si dopant layer is located 20 nm above the 2DEG. Both devices are fabricated simultaneously, with identical gate geometries. Note that S4 does not require the global-accumulation gate, but the design of the fine gates is similar to that shown in Fig. 1(e). The QDs are tuned to the Coulomb-blockade regime and we monitor the Coulomb oscillations as a function of time. Figure 2(a) shows that S1 is extremely stable over time. On the other hand, S4 shows a drift and jumps in the peak position, associated with charge instabilities in the device [Fig. 2(b)]. We observe similar characteristics in a variety of doped wafers and here only present data from the most promising QD. In contrast, we show here that stable QDs can be reliably fabricated in undoped heterostructures, irrespective of the 2DEG depth or the specific QD design.

In Fig. 3, we plot G as a function of the bias voltage (V_b) and the plunger gate voltage (V_P) for devices S1–S3. S1 is a double-layer QD in a deep (40 nm) 2DEG, and S2 (S3) are double- (single-)layer QDs fabricated on a shallow (10 nm) 2DEG. The charge-stability diagrams (typically acquired over several hours) are devoid of charge jumps and show well-defined Coulomb diamonds. Transport through excited states is visible in the form of conductance peaks running parallel to the diamond edges. We also observe regions with a negative differential conductance (particularly clear for S1), possibly arising from suppressed transport through specific excited states of the QD [32]. From the size of the smallest diamond, we estimate charging energies E_c of 1.23 meV (S1), 0.5 meV (S2),
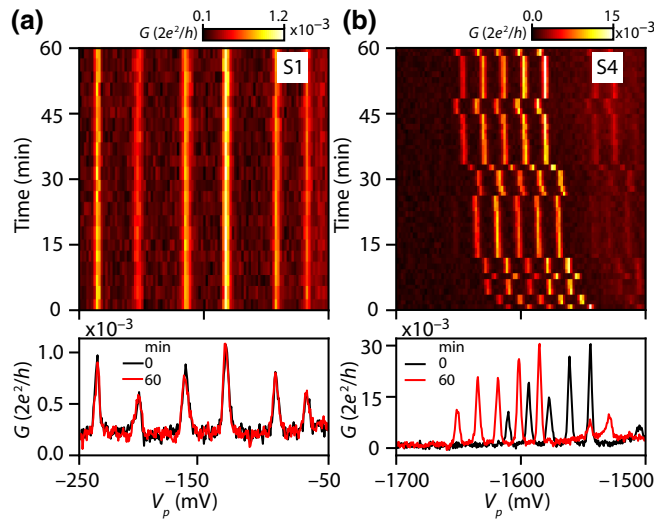
FIG. 2. (a) Top: the stability of the Coulomb oscillations as a function of time for an undoped wafer, sample S1. Bottom: the line cuts for $t = 0$ (black) and $t = 60$ (red) minutes. Gate settings: $V_L = -202$ mV, $V_R = -252$ mV, $V_C = -145$ mV, and $V_A = +500$ mV. (b) The same measurement for the doped wafer, sample S4. Gate settings: $V_L = -1600$ mV, $V_R = -1500$ mV, and $V_C = -1630$ mV.
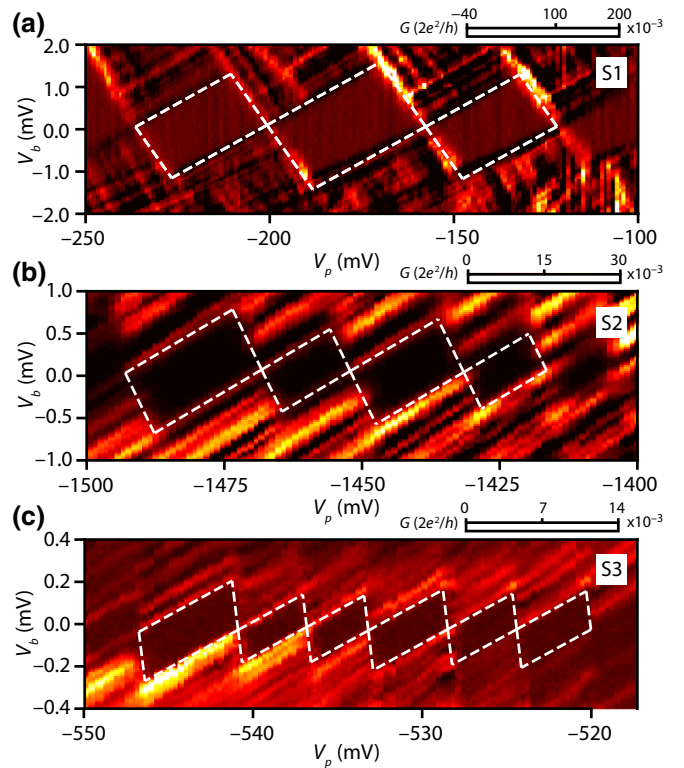

FIG. 3. Charge-stability diagrams for (a) S1, (b) S2, and (c) S3. Coulomb-blockaded regions are highlighted with white dashed lines and are used to estimate the charging energies.

and 0.16 meV (S3). These values are in good agreement with the designed geometries (for estimates of the QD size, see the Supplemental Material [23]). To fully characterize the dots, we also perform detailed gate-versus-gate measurements for different combinations of gates for each of the devices (shown in the Supplemental Material [23]). For double-layer dots, the left and right gates couple to the QD equally (corresponding capacitance ratios are $C_L/C_R \approx$ 0.9 for S1 and $C_L/C_R \approx 1$ for S2) and more strongly than the plunger gate ($C_L/C_P \approx 3.8$ for S1 and $C_L/C_P \approx 2.6$ for S2). For the single-layer dot S3, the tunnel gate T, with tips only in the vicinity of the active region, has smaller coupling compared to the plunger gate, $C_T/C_P \approx 0.6$. These coupling ratios agree with expectations from the respective QD designs, confirming the realization of well-defined quantum confinement.

The stability diagram in Fig. 3(a) also reveals an even-odd variation in the diamond size for S1, consistent with the spin-dependent filling of the orbital levels [17,33,34]. The low effective mass in InSb 2DEGs [13,35] allows us to observe this effect in relatively large QDs [36]. We confirm the alternating spin filling by studying the response of Coulomb peaks to a magnetic field applied in the plane of the 2DEG ($B_\parallel$). In Fig. 4(a), we show the magnetic field evolution of five Coulomb-blockade peaks for S1 from $B_\parallel = -0.2$ T to 0.6 T. The corresponding GSs are labeled A–D and peak positions (indicated by white dashed lines) are determined by fitting a Gaussian function. We note that the gate configuration here is different as compared to Fig. 3(a). The corresponding diamonds are presented

in the Supplemental Material [23]. At low fields between -0.2 and 0.2 T, successive Coulomb peaks move in opposite directions. This is consistent within the noninteracting picture, where the consecutive filling of electrons is based on the Pauli exclusion principle. Starting with an empty level, the first electron fills with a spin up or down and then the second electron fills the same state with the opposite spin. In this case, one expects two consecutive Coulomb-blockade peaks to move apart with an increasing Zeeman field. However, when the next electron enters the dot, it has to occupy a higher quantum level. Therefore, for two consecutive electrons belonging to different quantum levels, the corresponding peaks move toward each other as the field increases.

Figure 4(a) can also be represented in terms of the addition energy, defined as the difference in chemical potential (μ) between successive GS transitions, i.e., $\Delta\mu = \mu_{N+1} - \mu_N$. This value can be extracted directly from the Coulomb peak spacing by converting the gate voltage to energy using the plunger lever arm (see the Supplemental Material [23]). As shown in Fig. 4(b), a linear region is observed with an addition energy proportional to the Zeeman term, $\pm g\mu_B B$, where the sign depends on the parity of the GS. This allows us to extract the absolute value of the g factor, which lies in the range 26–35 for the four GSs analyzed here. At higher magnetic fields ($B_\parallel \simeq 0.3$ T), states B
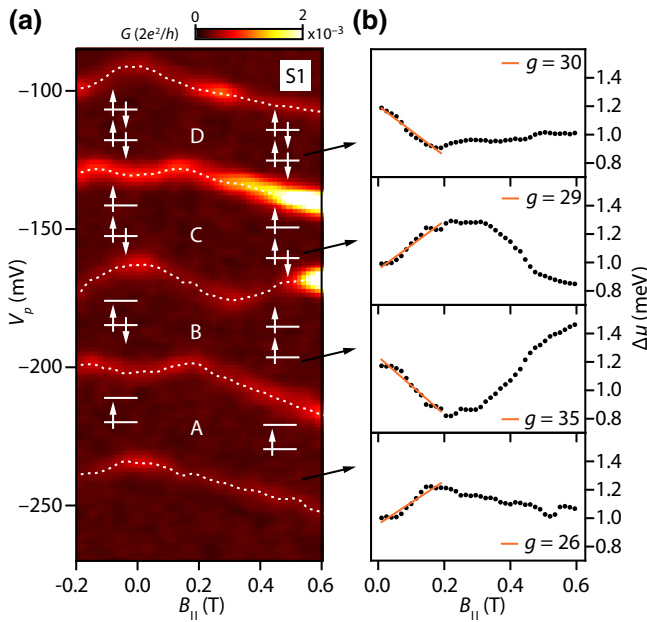
FIG. 4. (a) The evolution of the Coulomb-blockade peaks for S1 as a function of the in-plane magnetic field $B_{||}$. White dashed lines mark the peak positions and arrows represent the GS spin configuration. (b) The extracted addition energy as a function of $B_{||}$. The *g* factor is extracted from a linear fit (orange line) in the low-field regime.

and C display an overturned behavior, corresponding to a triplet GS with a total spin of 1, rather than a singlet state with a total spin of zero. This singlet-to-triplet transition is expected when the Zeeman energy is comparable to the singlet-triplet gap at the zero field [3,17,34,37]. It is worth noting that the large *g* factor of InSb 2DEGs allows for the observation of these GS transitions at significantly lower magnetic fields than for many other material systems [34,38–40].

In conclusion, we demonstrate the successful realization of stable controllable QDs in InSb 2DEGs. This stability allows us to fully characterize dots fabricated using two distinct designs. We show that the low effective mass leads to spin-dependent filling of the quantum levels for relatively large QDs. Furthermore, we extract a large Landé *g* factor (approximately 30), which results in a singlet-triplet transition at low magnetic fields. Our studies show that InSb quantum wells are an excellent platform for the study of quantum confined systems and are particularly relevant for future applications in topological superconductivity.

Datasets presented in this study are available online [41].

ACKNOWLEDGMENTS

[1] L. P. Kouwenhoven, C. M. Marcus, P. L. McEuen, S. Tarucha, R. M. Westervelt, and N. S. Wingreen, in *Mesoscopic Electron Transport*, edited by L. L. Sohn, L. P. Kouwenhoven, and G. Schön (Springer, Dordrecht, 1997), p. 105.

[2] S. M. Reimann and M. Manninen, Electronic structure of quantum dots, Rev. Mod. Phys. **74**, 1283 (2002).

[3] R. Hanson, L. P. Kouwenhoven, J. R. Petta, S. Tarucha, and L. M. K. Vandersypen, Spins in few-electron quantum dots, Rev. Mod. Phys. **79**, 1217 (2007).

[4] D. Loss and D. P. DiVincenzo, Quantum computation with quantum dots, Phys. Rev. A **57**, 120 (1998).

[5] J. R. Petta, A. C. Johnson, J. M. Taylor, E. A. Laird, A. Yacoby, M. D. Lukin, C. M. Marcus, M. P. Hanson, and A. C. Gossard, Coherent manipulation of coupled electron spins in semiconductor quantum dots, Science **309**, 2180 (2005).

[6] M. Veldhorst, C. H. Yang, J. C. C. Hwang, W. Huang, J. P. Dehollain, J. T. Muhonen, S. Simmons, A. Laucht, F. E. Hudson, K. M. Itoh, A. Morello, and A. S. Dzurak, A two-qubit logic gate in silicon, Nature **526**, 410 (2015).

[7] T. Byrnes, N. Y. Kim, K. Kusudo, and Y. Yamamoto, Quantum simulation of Fermi-Hubbard models in semiconductor quantum-dot arrays, Phys. Rev. B **78**, 075320 (2008).

[8] E. Manousakis, A quantum-dot array as model for copper-oxide superconductors: A dedicated quantum simulator for the many-fermion problem, J. Low Temp. Phys. **126**, 1501 (2002).

[9] T. Hensgens, T. Fujita, L. Janssen, X. Li, C. J. Van Diepen, C. Reichl, W. Wegscheider, S. Das Sarma, and L. M. K. Vandersypen, Quantum simulation of a Fermi-Hubbard model using a semiconductor quantum dot array, Nature **548**, 70 (2017).

[10] J. D. Sau and S. D. Sarma, Realizing a robust practical majorana chain in a quantum-dot-superconductor linear array, Nat. Commun. **3**, 964 (2012).

[11] T. Karzig, C. Knapp, R. M. Lutchyn, P. Bonderson, M. B. Hastings, C. Nayak, J. Alicea, K. Flensberg, S. Plugge, Y. Oreg, C. M. Marcus, and M. H. Freedman, Scalable designs for quasiparticle-poisoning-protected topological quantum computation with Majorana zero modes, Phys. Rev. B **95**, 235305 (2017).

[12] S. Plugge, A. Rasmussen, R. Egger, and K. Flensberg, Majorana box qubits, New J. Phys. **19**, 012001 (2017).

[13] Z. Lei, C. A. Lehner, E. Cheah, M. Karalic, C. Mittag, L. Alt, J. Scharnetzky, W. Wegscheider, T. Ihn, and K. Ensslin, Quantum transport in high-quality shallow InSb quantum wells, Appl. Phys. Lett. **115**, 012101 (2019).

[14] F. Qu, J. Van Veen, F. K. De Vries, A. J. A. Beukman, M. Wimmer, W. Yi, A. A. Kiselev, B. M. Nguyen, M. Sokolich, M. J. Manfra, F. Nichele, C. M. Marcus, and L. P. Kouwenhoven, Quantized conductance and large *g*-factor

anisotropy in InSb quantum point contacts, Nano Lett. **16,** 7509 (2016).

[15] R. L. Kallaher, J. J. Heremans, N. Goel, S. J. Chung, and M. B. Santos, Spin-orbit interaction determined by antilocalization in an InSb quantum well, Phys. Rev. B **81,** 075303 (2010).

[16] B. Nedniyom, R. J. Nicholas, M. T. Emeny, L. Buckle, A. M. Gilbertson, P. D. Buckle, and T. Ashley, Giant enhanced *g*-factors in an InSb two-dimensional gas, Phys. Rev. B **80,** 125328 (2009).

[17] H. A. Nilsson, P. Caroff, C. Thelander, M. Larsson, J. B. Wagner, L.-E. Wernersson, L. Samuelson, and H. Q. Xu, Giant, level-dependent *g* factors in InSb nanowire quantum dots, Nano Lett. **9,** 3151 (2009).

[18] S. Nadj-Perge, V. S. Pribiag, J. W. G. Van Den Berg, K. Zuo, S. R. Plissard, E. P. A. M. Bakkers, S. M. Frolov, and L. P. Kouwenhoven, Spectroscopy of Spin-Orbit Quantum Bits in Indium Antimonide Nanowires, Phys. Rev. Lett. **108,** 166801 (2012).

[19] I. van Weperen, B. Tarasinski, D. Eeltink, V. S. Pribiag, S. R. Plissard, E. P. A. M. Bakkers, L. P. Kouwenhoven, and M. Wimmer, Spin-orbit interaction in InSb nanowires, Phys. Rev. B **91,** 201413 (2015).

[20] J. Xue, Y. Chen, D. Pan, J.-Y. Wang, J. Zhao, S. Huang, and H. Q. Xu, Gate defined quantum dot realized in a single crystalline InSb nanosheet, Appl. Phys. Lett. **114,** 023108 (2019).

[21] J. M. S. Orr, P. D. Buckle, M. Fearn, C. J. Storey, L. Buckle, and T. Ashley, A surface-gated InSb quantum well single electron transistor, New J. Phys. **9** (2007).

[22] T. Masuda, K. Sekine, K. Nagase, K. S. Wickramasinghe, T. D. Mishima, M. B. Santos, and Y. Hirayama, Transport characteristics of InSb trench-type in-plane gate quantum point contact, Appl. Phys. Lett. **112,** 192103 (2018).

[23] See the Supplemental Material at http://link.aps.org/supplemental/10.1103/PhysRevApplied.13.041003 for wafer characterization, fabrication details, and additional device measurements.

[24] W. Yi, A. A. Kiselev, J. Thorp, R. Noah, B.-M. Nguyen, S. Bui, R. D. Rajavel, T. Hussain, M. F. Gyure, P. Kratz, Q. Qian, M. J. Manfra, V. S. Pribiag, L. P. Kouwenhoven, C. M. Marcus, and M. Sokolich, Gate-tunable high mobility remote-doped InSb/In$_{1-x}$Al$_x$Sb quantum well heterostructures, Appl. Phys. Lett. **106,** 142103 (2015).

[25] T.-M. Lu, N. Bishop, T. Pluym, J. Means, P. G. Kotula, J. Cederberg, L. A. Tracy, J. Dominguez, M. P. Lilly, and M. S. Carroll, Enhancement-mode buried strained silicon channel quantum dot with tunable lateral geometry, Appl. Phys. Lett. **99,** 043101 (2011).

[26] M. G. Borselli, K. Eng, E. T. Croke, B. M. Maune, B. Huang, R. S. Ross, A. A. Kiselev, P. W. Deelman, I. Alvarado-Rodriguez, A. E. Schmitz, M. Sokolich, K. S. Holabird, T. M. Hazard, M. F. Gyure, and A. T. Hunter, Pauli spin blockade in undoped Si/SiGe two-electron double quantum dots, Appl. Phys. Lett. **99,** 1 (2011).

[27] N. Hendrickx, D. Franke, A. Sammak, M. Kouwenhoven, D. Sabbagh, L. Yeoh, R. Li, M. Tagliaferri, M. Virgilio, G. Capellini, G. Scappucci, and M. Veldhorst, Gate-controlled quantum dots and superconductivity in planar germanium, Nat. Commun. **9,** 2835 (2018).

[28] X. Gong, T. Yamaguchi, H. Kan, T. Makino, K. Ohshimo, M. Aoyama, M. Kumagawa, N. Rowell, and R. Rinfret, Sulphur passivation of InAs(Sb), Appl. Surf. Sci. **113–114,** 388 (1997).

[29] H. Zhang *et al.*, Ballistic superconductivity in semiconductor nanowires, Nat. Commun. **8,** 16025 (2017).

[30] M. M. Uddin, H. W. Liu, K. F. Yang, K. Nagase, K. Sekine, C. K. Gaspe, T. D. Mishima, M. B. Santos, and Y. Hirayama, Gate depletion of an InSb two-dimensional electron gas, Appl. Phys. Lett. **103,** 123502 (2013).

[31] M. Ciorga, A. S. Sachrajda, P. Hawrylak, C. Gould, P. Zawadzki, S. Jullian, Y. Feng, and Z. Wasilewski, Addition spectrum of a lateral dot from Coulomb and spin-blockade spectroscopy, Phys. Rev. B **61,** R16315 (2000).

[32] J. Weis, R. J. Haug, K. V. Klitzing, and K. Ploog, Competing Channels in Single-Electron Tunneling Through a Quantum Dot, Phys. Rev. Lett. **71,** 4019 (1993).

[33] D. H. Cobden and J. Nygård, Shell Filling in Closed Single-Wall Carbon Nanotube Quantum Dots, Phys. Rev. Lett. **89,** 046803 (2002).

[34] C. Fasth, A. Fuhrer, L. Samuelson, V. N. Golovach, and D. Loss, Direct Measurement of the Spin-Orbit Interaction in a Two-Electron InAs Nanowire Quantum Dot, Phys. Rev. Lett. **98,** 266801 (2007).

[35] C. T. Ke, C. M. Moehle, F. K. de Vries, C. Thomas, S. Metti, C. R. Guinn, R. Kallaher, M. Lodari, G. Scappucci, T. Wang, R. E. Diaz, G. C. Gardner, M. J. Manfra, and S. Goswami, Ballistic superconductivity and tunable π junctions in InSb quantum wells, Nat. Commun. **10,** 3764 (2019).

[36] Y. M. Blanter, A. D. Mirlin, and B. A. Muzykantskii, Fluctuations of Conductance Peak Spacings in the Coulomb Blockade Regime: Role of Electron-Electron Interaction, Phys. Rev. Lett. **78,** 2449 (1997).

[37] F. Deon, V. Pellegrini, F. Carillo, F. Giazotto, G. Biasiol, L. Sorba, and F. Beltram, Singlet-triplet transition in a few-electron lateral In$_{0.75}$Ga$_{0.25}$As/In$_{0.75}$Al$_{0.25}$As quantum dot, Appl. Phys. Lett. **96,** 142107 (2010).

[38] R. M. Potok, J. A. Folk, C. M. Marcus, V. Umansky, M. Hanson, and A. C. Gossard, Spin and Polarized Current from Coulomb Blockaded Quantum Dots, Phys. Rev. Lett. **91,** 016802 (2003).

[39] G. Katsaros, P. Spathis, M. Stoffel, F. Fournel, M. Mongillo, V. Bouchiat, F. Lefloch, A. Rastelli, O. Schmidt, and S. De Franceschi, Hybrid superconductor-semiconductor devices made from self-assembled SiGe nanocrystals on silicon, Nat. Nanotechnol. **5,** 458 (2010).

[40] A. Kurzmann, M. Eich, H. Overweg, M. Mangold, F. Herman, P. Rickhaus, R. Pisoni, Y. Lee, R. Garreis, C. Tong, K. Watanabe, T. Taniguchi, K. Ensslin, and T. Ihn, Excited States in Bilayer Graphene Quantum Dots, Phys. Rev. Lett. **123,** 026803 (2019).

[41] I. Kulesh, C. T. Ke, C. Thomas, S. Karwal, C. M. Moehle, S. Metti, R. Kallaher, G. C. Gardner, M. J. Manfra, and S. Goswami, Dataset for: "Quantum dots in an InSb two-dimensional electron gas," https://doi.org/10.4121/uuid:28a121af-1e08-429d-9d53-1cc53764e91e (2020).